SIMULATION OF SPACE-CHARGE COMPENSATION OF A LOW-ENERGY PROTON BEAM IN A DRIFT SECTION

Daniel Noll*, Martin Droba, Oliver Meusel, Ulrich Ratzinger, Kathrin Schulte

Institute for Applied Physics, Goethe University, Frankfurt am Main, Germany

Abstract

Space-charge compensation provided by the accumulation of particles of opposing charge in the beam potential is an important effect occuring in magnetostatic low energy beam transport sections of high-intensity accelerators. An improved understanding of its effects might provide valuable input for the design of these beam lines.

One approach to model the compensation process are Particle-in-Cell (PIC) simulations including residual gas ionisation. In simulations of a drifting proton beam, using the PIC code *bender* [1], some features of thermal equilibrium for the compensation electrons were found. This makes it possible to predict their spatial distribution using the Poisson-Boltzmann equation and thus the influence on beam transport.

In this contribution, we will provide a comparison between the PIC simulations and the model as well as some ideas concerning the source of the (partial) thermalization.

SIMULATION OF A DRIFT SECTION

The drift of a 120 keV, 100 mA proton beam over 50 cm through a system enclosed by repeller electrodes on -1.5 kV and filled with Argon gas at 1×10^{-5} mbar was simulated. The code *bender*, the simulation model, the reasons for the choice of this system as well as the behaviour during compensation build-up were presented in previous contributions [1, 2].

Figure 1 depicts the charge densities of all simulated species – the beam protons, the residual gas ions (Ar^{1+}) and the compensation electrons – in the steady-state of the simulation. The globally averaged compensation outside of the area affected by the repellers reaches $\eta_{part} \approx 86.2\,\%$. Beyond the mean effect of the compensation, a shift in the focus of the beam, which is also easily explained by a scaling of the current, some additional effects are present.

In the focus, the beam becomes hollow. As can be observed in the total charge density, the beam edge is not well compensated, especially in the focus point but also elsewhere in the system. Some electrons have enough energy to be able to form an area of negative charge density close to the beam edge. In most parts of the system, the residual gas ions are immediately expelled by the radial electric field. However, within the focus, the Argon ions accumulate to a density of approximately $300\,\mu C\,m^{-3}$ – surprising, since the radial electric fields should be largest in the focus.

Figure 2 shows the distribution of total particles energies H in arbitrarily selected places throughout the volume. For
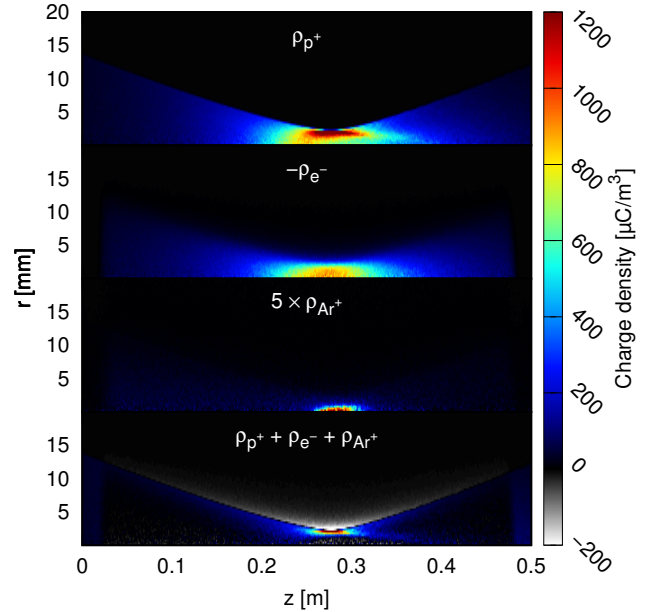

Figure 1: Charge densities for the different particle species in the simulation: beam protons, compensation electrons, residual gas ions and the netto charge density.
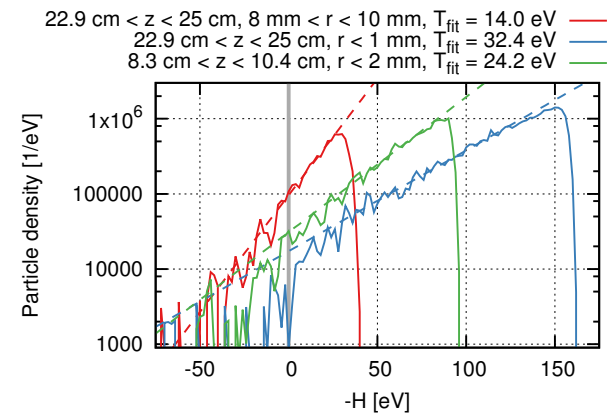

Figure 2: Distribution of total particle energy H (kinetic plus potential energy) at various arbitrarily chosen positions. For $H < 0$, the curves follow the dashed exponential curves. Positive H are underpopulated due to particle loss.

$H < 0$, these follow an exponential dependence

$$H(r, v) = H_0 \exp(-H/(k_b T))$$
$$= H_0 \exp\left(-p^2/(2m_e k_b T) + e\varphi(r)/(k_b T)\right). \quad (1)$$

For $H \geq 0$, particles are not confined and are gradually lost, leading to an underpopulation. The Boltzmann distribu-

---
* noll@iap.uni-frankfurt.de

tion in Eq. (1) also predicts Gaussian velocity distributions. These were also observed in the simulation. An example, resolved radially, taken from the center of the system is shown in Fig. 3. Towards larger radii, their width decreases and the curves look more "cut-off", probably due to particle losses.
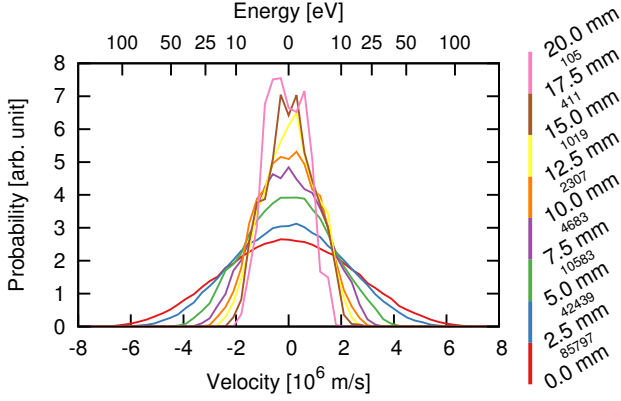

Figure 3: Electron velocities in a slice around $z = 25$ cm resolved radially and normalized independently. The small numbers in the caption give the number of macroparticles contained in each ring.

Therefore, the results show some features of a system in thermal equilibrium. But neither is there equipartitioning – the temperatures differ between the transversal and the longitudinal plane – nor are the temperatures constant spatially. Nevertheless, the assumption that the electrons distribute according to Eq. (1) allows us to understand the features previously found in Fig. 1.

POISSON-BOLTZMANN EQUATION

When the electrons are known to be Boltzmann distributed, their distribution in space can be found by solving

$$\nabla^2 \varphi(r) = -\frac{1}{\epsilon_0}\left(\rho_{\text{beam}}(r) + \rho_{\text{comp}} \exp\left(\frac{e\varphi(r)}{k_b T}\right)\right).$$

By scaling the coordinates by the Debye length $\lambda_d = \sqrt{\epsilon_0 k_b T/(ne^2)}$ and the potential by the temperature, $\tilde{\phi} = e\phi/(k_b T)$, [3] we get

$$\tilde{\nabla}^2 \tilde{\varphi} = f_{\text{beam}}(\tilde{r}) - \mu \exp(\tilde{\varphi}), \qquad (2)$$

where $f_{\text{beam}}(\tilde{r}) = \rho_{\text{beam}}(\tilde{r})/(ne)$ is the beam profile. λ_d and the compensation degree incorporated in

$$\mu = \eta_{\text{part}} \int \exp(\tilde{\varphi}(r))\, \mathrm{d}V \left(\int f_{\text{beam}}(r)\, \mathrm{d}V\right)^{-1},$$

are the only free parameters of the model. Equation (2) can be solved by introducing a parameter t,

$$\frac{\mathrm{d}\varphi}{\mathrm{d}t} = \tilde{\nabla}^2 \tilde{\varphi} - f_{\text{beam}}(\tilde{r}) + \mu \exp \tilde{\varphi}(\tilde{r})$$

and applying the Crank-Nicolson method [4, p. 1045] for the linear terms on the right hand side and the forward Euler method for the exponential term.
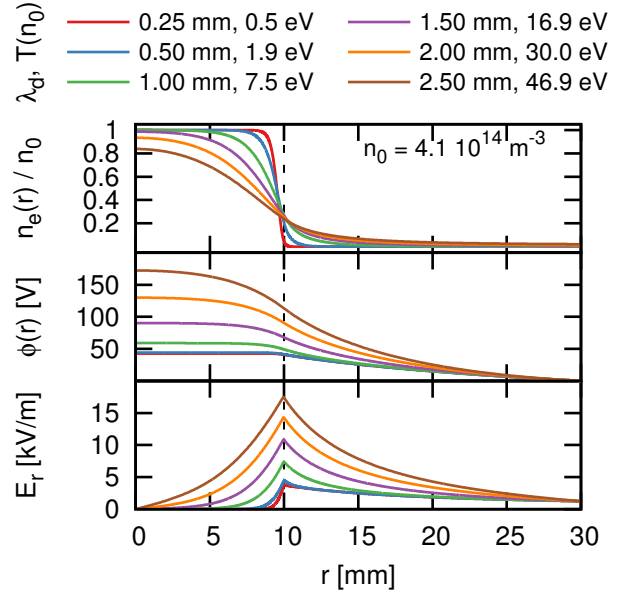

Figure 4: Electron density n_e relative to the beam density n_0, remaining potential ϕ and electric field, when electrons at temperature T confined in a 100 mA, 120 keV proton beam are treated using Eq. (2). Compensation degree is 90 %.

Figure 4 displays the electron density, potential and electric field found from the solution of Eq. (2) for a 100 mA, 120 keV proton beam with 1 cm radius, compensated to $\eta_{\text{part}} = 90\,\%$ by thermal electrons. The algorithm was also included into the beam transport code *tralitrala* as a space-charge solver to be able to look at the influence of the non-linear fields produced by the electrons. Figure 5 shows the emittance growth observed in a 50 cm drift of an initially parallel and homogeneous 50 mA, 120 keV proton beam ($\epsilon_{\text{rms}} = 25$ mm mrad, $\alpha = 0$, $\beta = 1$ m).

For low temperatures, the electrons are concentrated around the beam axis and are able to fully compensate the beam within some radius. The charge density effectively becomes that of a hollow beam, i.e. the electric field is zero in the core of the beam and rises quadratically at the edge. Such a situation does not lead to emittance growth, when the beam is either close to fully or not compensated. However, at intermediate values of η_{part}, where the quadratic electric field affects a large part of the beam, a growth in emittance up to 15 % can be observed.

For higher temperatures, the radial electron density begins to decrease earlier, leading to some electric field over a wide part of the beam. This produces some emittance growth, but not as large as for very low temperatures. Additionally more and more electrons are located outside the beam radius, leading to the negative charge densities also observed in the *bender* simulation.

At very large temperatures, the electron distribution tends towards a homogeneous background, providing nearly no effective compensation but also not leading to any emittance growth. Such a situation is unlikely to occur, since electron losses on the beam pipe would become too large.
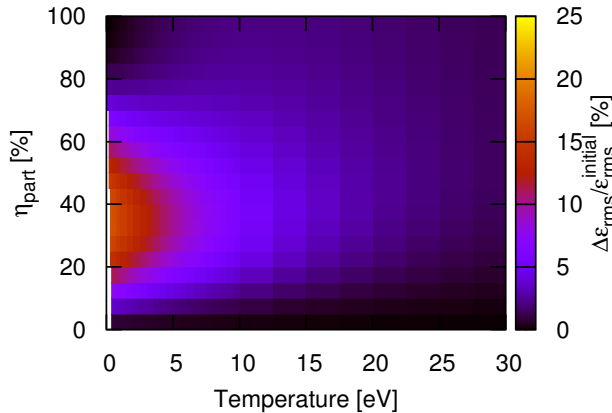
Figure 5: Emittance growth in a 50 cm beam transport of a homogeneous beam, when electrons at given temperature and compensation degree are incorporated in the simulation. Source of the emittance growth are the non-linear fields observed in Fig. 4.
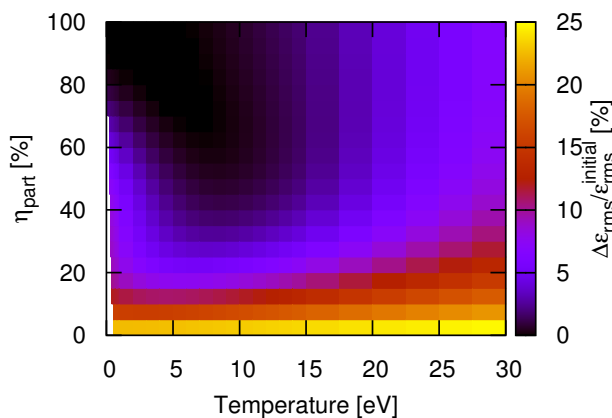

Figure 6: Same parameters as Fig. 5, but for a beam with a Gaussian distribution.

Simulations with rms equivalent parameters were made for a beam with a Gaussian distribution in phase-space. Figure 6 shows the calculated emittance growth. The largest growth is observed for an uncompensated beam, which is a result of redistribution due to non-linear field energy. In the presence of a small number of electrons, the growth is much reduced. In Fig. 6 for example, $\Delta\epsilon_{rms}/\epsilon_{rms} < 10\%$, for $\eta_{part} > 40\%$ over the length of the drift. Around $\eta_{part} = 60\%$, $T = 8$ eV, the electrons distribute in a way that the resulting electric field is approximately linear. This leads to the surprising minimum in the emittance growth.

Figure 7 shows the charge density from a similar calculation of the system previously simulated using *bender*. The properties $T(z)$ and $\eta_{part}(z)$ of the electrons were extracted from the full simulation, but their radial distribution calculated from Eq. (2).
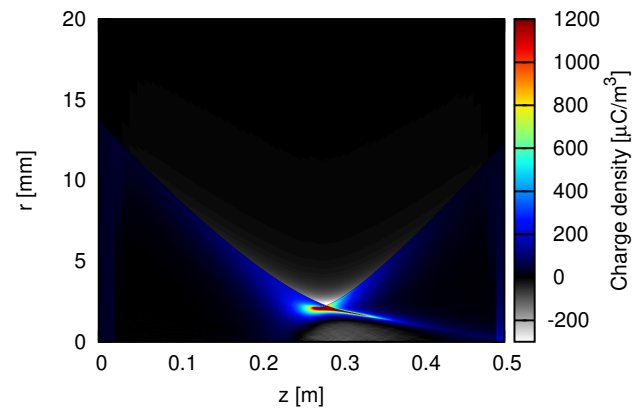

Figure 7: Total charge density in a 2d simulation of the same system as in Fig. 1, when electric fields are calculated from Eq. (2) using the same temperature $T(z)$ and longitudinal compensation degree distribution $\eta_{part}(z)$ extracted from the full simulation.

Both the formation of the negative charge density beyond the beam edge as well as the formation of a hollow beam is present. The latter can be identified as a result of the sharp increase of the electric field at the edge of the beam. This reduces the angle of convergence for the particles leading to an increase in density after some drift. Beyond the focus point, these areas are still observed continuing towards the axis.

The Poisson-Boltzmann model does not include the secondary ions. This makes it possible for a negative charge density to form inside the area around $z = 30$ cm close to the beam axis. In this area, in the *bender* simulation, residual gas ions are not accelerated from the system anymore but confined instead.

Therefore, all features previously identified in the PIC simulation can be explained by the presence of Boltzmann distributed electrons. Hence, the question of its origin becomes important.

STOCHASTICAL HEATING IN A TEST SYSTEM

In the PIC simulation, we observed that the energies of the electrons fluctuate randomly, over a scale of several electron-volts in short-term, but on average increasing continously. When their kinetic energy increases to values larger than the potential, these electrons are lost. Due to this, we suspected that energy is not conserved by the simulation.

To test this hypothesis, a test system was generated by solving Eq. (2) in spherical coordinates for a confining potential of Gaussian shape with $\sigma = 1$ cm. The resulting charge density is displayed in Fig. 8. To avoid particle loss, the system parameters were chosen so that the confined particles are well removed from the boundary of the system, taken to be at $R = 10$ cm. Particle distributions with a thermal energy distribution and the calculated densities profile were

then loaded into *bender* and simulated for up to 1.5 ms (30 million steps) in some cases.
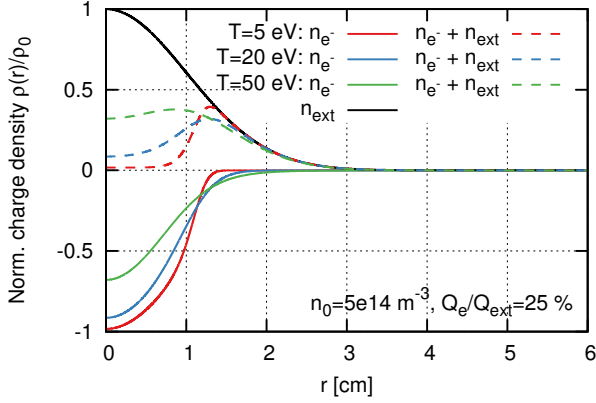

Figure 8: Electron charge density in a Gaussian shaped confining potential for various temperatures.

The density profile should remain stable by design. At a high number of particles, this was also observed. For low-resolution simulations however, a slow increase in the size of the cloud is present. The origin of this expansion is the linear increase in average particle energy shown in Fig. 9.
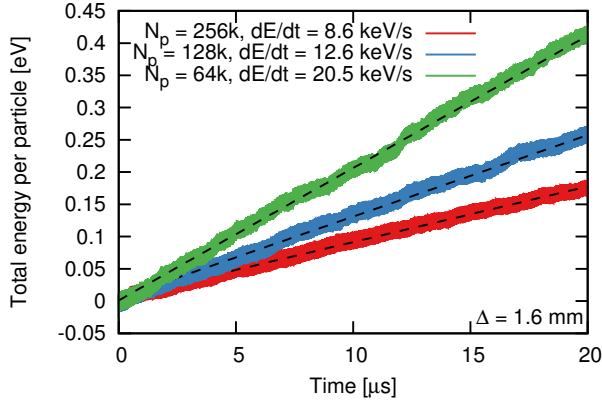

Figure 9: Energy increase in the test system (see Fig. 8) due to stochastical heating.

The rate of energy increase mainly depends on the number of macroparticles used and to a lesser degree on the resolution of the simulation grid. A range of parameters were simulated and the corresponding energy increase rate displayed in Fig. 10.

A possible explanation for the heating can be found in [5, p. 314-318]. Repeating their argument, if we assume that all errors in the simulation contribute to a random error δE in the electric field that has zero time average $\overline{\delta E} = 0$ but a variance $\overline{\delta E^2} \neq 0$, then the kinetic energy change in the simulation between two timesteps is

$$\Delta T = T_{i+1} - T_i = \frac{1}{2}m\left(\overline{(v_i + \delta v)^2} - \overline{v_i^2}\right) \quad (3)$$

$$= \frac{1}{2}m\left(2v_i\overline{\delta v} + \overline{\delta v^2}\right) = \frac{1}{2}\frac{q^2}{m}\overline{\delta E^2}\delta t^2. \quad (4)$$
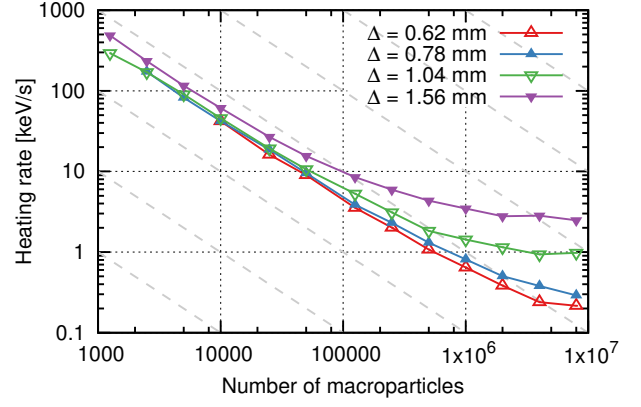

Figure 10: Observed heating rate for different numbers of macroparticles and grid spacings Δ. Dashed lines indicate $O(N^{-1})$ behaviour.

Equation 4 therefore predicts a constant increase in energy, which is what is observed. For a low number of macroparticles, we can assume the error to be statistical and therefore $|\delta E| \sim 1/\sqrt{N}$. Then, the heating rate is inversely proportional to the number of macroparticles N. This is observed in Fig. 10. Depending on the grid resolution at some point, some other (unidentified) process becomes relevant.

Therefore, we can assume a numerical heating to be present in the simulation, with a heating rate dependent on the parameters of the simulation.

In hindsight, the choice of system was not ideal, because a dependence on plasma parameters such as the Debye length is hard to find given the small extent of the system.

NUMERICAL INFLUENCES IN THE DRIFT SIMULATION

Figure 11 shows the temperatures found in the drift system, when the number of beam macroparticles inserted per step (and therefore the charge per macroparticle) is changed. As the electron temperature decreases, more electrons remain closer to the beam axis and the amount of negative charge outside the beam is lower. This allows more electrons to accumulate. Therefore, the decrease in temperature is linked to an increase in total compensation degree of the system. This can be seen in Fig. 11.

We assume that the observed dependence on the number of macroparticles is a result of the stochastical heating previously observed in the demonstration system. Due to particle losses, instead of a continous increase of system energy, an equilibrium forms. The losses could then also be responsible for the appearance of the Boltzmann energy distribution.

When the electric field of the beam is not recalculated in every step from beam particles but fixed to a field taken from a previous simulation, the observed (transversal) temperatures at the center of the system shrink from 27 eV to 11.8 eV. When residual gas ions are also excluded, the results is 8.3 eV. Therefore, a significant contribution of the heating comes from the beam particles.
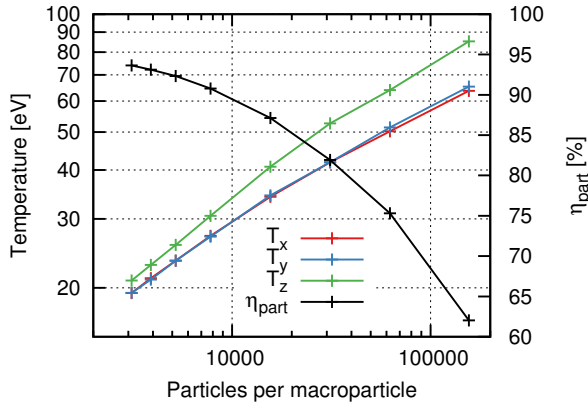
Figure 11: Dependence of the observed electron temperatures and the compensation degree on the number of macroparticles used to represent the particle species in the *bender* simulation.

To make the results of this kind of simulation physical, the numerical heating needs to be removed by some means. We then expect the compensation degree to reach values close to 100 %.

Then, physical heating processes such as Coulomb collisions between beam particles and the compensation electrons can be introduced. An estimation for the heating from these collision, given by Doelling [6, p. 19],

$$ P = \frac{e^2}{4\pi\epsilon_0^2 m_e} \frac{n_b q_b^2}{v_b} \ln(\Lambda) \left[\mathrm{erf}\left(\frac{v_b}{v_t}\right) \right. $$
$$ \left. - \frac{2}{\sqrt{\pi}} \left(1 + \frac{m_e}{m_b}\right) \frac{v_b}{v_t} \exp\left(-\left(\frac{v_b}{v_t}\right)^2\right) \right], $$

$v_t = \sqrt{2k_b T/m_e}$, indicates that for exemplary parameters taken from the simulation ($T = 25\,\mathrm{eV}$), the heating rate $P = 19.5\,\mathrm{keV\,s^{-1}}$ is in the same order of magnitude of the numerical heating described in the previous section. Therefore, final results may, in some ways, not deviate much from those with the unphysical heating.

CONCLUSION

Simulations of space charge compensation in a short drift section were performed using the newly-developed Particle-in-Cell code *bender*. Beyond the reduction in space-charge forces, several features such as the formation of a hollow beam or the accumulation of residual gas ions in the focus were found. These were linked to the presence of a Boltzmann energy distribution for the electrons. Results from simulation using different simulation parameters and from a numerical experiment indicate that the observed energy distributions are of numerical origin.

REFERENCES

[1] D. Noll, M. Droba, O. Meusel, U. Ratzinger, K. Schulte and C. Wiesner, "The Particle-in-Cell Code Bender and Its Application to Non-Relativistic Beam Transport", in Proc. HB2014, East Lansing, USA, November 2014, paper WEO4LR02, pp. 304-308.

[2] D. Noll, M. Droba, O. Meusel, U. Ratzinger, K. Schulte and C. Wiesner, "Investigation of Space-Charge Compensation in Low-Energy Beam Transport (LEBT) Sections Using a Particle-In-Cell Code", in Proc. LINAC2014, Geneva, Switzerland, September 2014, paper MOPP065, pp. 205-207.

[3] R. G. Lefrancois, T. S. Pedersen, A. H. Boozer and J.P. Kremer, "Numerical Investigation of Three-Dimensional Single-Species Plasma Equilibria on Magnetic Surfaces", Physics of Plasmas, 12, 072105 (2005).

[4] Press, H. P. et al., "Numerical Recipes", Cambridge University Press, 2007.

[5] R. W. Hockney and J. W. Eastwood, "Computer Simulation Using Particles", CRC Press, 1988.

[6] Dölling, R., "Raumladungskompensation driftender intensiver Strahlen niederenergetischer Ionen und Techniken zu ihrer Vermessung", Dissertation, Johann-Wolfgang Goethe Universität Frankfurt am Main, 1994.